Available online at www.sciencedirect.com

ScienceDirect

Ceramics International 40 (2014) 1303–1310

CERAMICS INTERNATIONAL

www.elsevier.com/locate/ceramint

Tough ceramics by microwave sintering of nanocrystalline titanium diboride ceramics

D. Demirskyi[a,b,c,*], D. Agrawal[b,1], A. Ragulya[c,2]

[a]National Institute for Materials Science, 1-2-1 Sengen, Tsukuba, Ibaraki 305-0047, Japan
[b]Materials Research Institute, The Pennsylvania State University, University Park, PA 10802, USA
[c]Frantsevich Institute for Problems in Material Science, 3 Krzhizhanovsky street, 03680 Kyiv, Ukraine

Received 13 June 2013; received in revised form 1 July 2013; accepted 1 July 2013
Available online 6 July 2013

Abstract

Dense composites of TiB_2 with additions of TiN have been produced by microwave sintering. Microwave sintering was conducted at 1200–1700 °C under controlled atmosphere. The effects of composition, sintering temperature, on densification, microstructure, and mechanical properties were investigated. Microwave sintering resulted in uniform crack-free uniform microstructure, as well as maximum relative density of 99% and bending strength of 368 ± 15 MPa, Young's modulus of 440 ± 11 GPa, electric resistivity of 2×10^{-5} Ω cm, Vickers hardness of 26.2 ± 0.4 GPa, and a fracture toughness of 6.2 ± 0.34 MPa · $m^{1/2}$ were obtained using 36 wt% TiB_2, and sintering for 10 min at 1650 °C.

Keywords: A. Sintering; Microwave heating; Ceramics; TiB_2; TiN

1. Introduction

Titanium diboride (TiB_2) is a refractory intermetallic compound with excellent hardness, corrosion resistance and electrical conductivity [1,2]. TiB_2 based ceramics have been studied extensively for cutting tools, and armor materials because of their exceptional mechanical properties under various service conditions [3]. It is difficult to sinter TiB_2 by standard heating methods because of its low self-diffusion rate. Therefore, most reported works on densification of TiB_2 have been done using advanced consolidation methods such as hot-pressing, spark-plasma sintering and microwave sintering [4–14].

Microwave sintering (MWS) is relatively a new method for processing of ceramics and metals and is generally associated with high heating rates and volumetric heating [15]. Microwave sintering ensures considerable time and energy saving, and therefore is viewed as one of the most prospective sintering techniques in material processing [15,16]. It has been shown that MWS may provide enhanced densification during sintering of oxides [17–19], metals [20–24] and non-oxide ceramics [25–28]. Processing of high-melting point compounds such as TiB_2 is very difficult due to the need of proper high temperature insulation and/or special design of microwave applicator [14]. Therefore in this study, the effect of TiN addition on homogeneity of heating process and sintering process under microwave radiation has been studied. An analysis of densification kinetics, microstructural evolution and mechanical properties of TiB_2 microwave sintered ceramics was conducted in this study.

2. Experimental procedure

2.1. Processing

For sintering experiments we used commercially available TiN (US-Nano, USA, BET = 58 $m^2 g^{-1}$, < 0.3 wt% O) TiB_2

*Corresponding author at: National Institute for Materials Science, 1-2-1 Sengen, Tsukuba-city, Ibaraki 305-0047, Japan. Tel.: +81 29 859 2461; fax: +81 29 859 2401.
E-mail addresses: demirskyi.dmytro@nims.go.jp (D. Demirskyi), dxa4@psu.edu (D. Agrawal), ragulya@ipms.kiev.ua (A. Ragulya).
[1]Tel.: +814 863 8034; fax: +814 865 2326.
[2]Tel.: +380 44 424 7435; fax: +380 44 424 21 31.

0272-8842/$ - see front matter © 2013 Elsevier Ltd and Techna Group S.r.l. All rights reserved.
http://dx.doi.org/10.1016/j.ceramint.2013.07.010

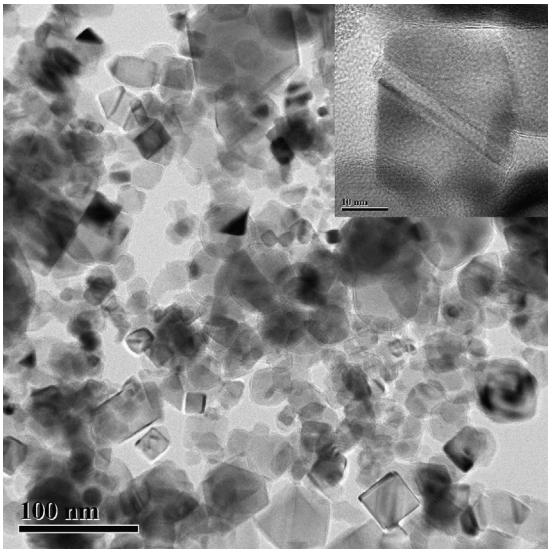

Fig. 1. TEM observation of the starting 50/50 wt% TiN–TiB_2 powder.

(US-Nano, USA, BET = 45 $m^2\,g^{-1}$, < 1.9 wt% O) powders, and TiN–TiB_2 plasma-synthesized composites with the composition of 64/36 and 50/50 wt% (Neomat, Latvia, BET = 28 $m^2\,g^{-1}$, < 1.0 wt% O) were used as starting materials. Typical powder morphology observed by TEM is shown in Fig. 1.

All available powder compositions were milled for 30 min at a milling rotation speed of 300 rpm, using ethanol and agate balls as a milling medium. The weight ratio of balls to powder was fixed to 5:1. The resultant slurry was dried in vacuum evaporator and screened through a 60 mesh screen.

The powders were cold compacted at a pressure of 150 MPa into pellets of 25 mm (~1 in.) in diameter and 5 mm in thickness. That was followed by cold isostatic pressing at 220 MPa. At this stage, samples had a green density of around 50% of the theoretical density.

Sintering experiments were carried out using a 6 kW, 2.45 GHz multimode microwave cavity. No additional susceptors were used in the experimental setup, so that the heating was pure microwave heating, detailed information of the experimental set-up is presented elsewhere [29]. The heating profile consisted of a heating rate of 50 °C min^{-1} from room temperature to 800 °C with a dwell time of 1 min to insure pyrometer (Raytek MA2SC) readings. The samples were then heated to the maximum temperature at 5, 20 and 50 °C min^{-1}. Sintering was performed between 1400 and 1650 °C for a set time of 10 min under pure flowing argon atmosphere and freely cooled down to room temperature.

2.2. Characterizations of sintered samples

Density of sintered samples was measured using the Archimedes' method (ASTM B963-08). Microstructural observations and analyses were carried out on polished sections using Jeol JSM-7001F field emission scanning electron microscope (SEM) equipped with an energy dispersive spectrometer. The average grain size was measured from SEM graphs using a line-intercept method, and taking into account of at least 100 grains (with a three-dimensional correction factor determined to be 1.2 (ASTM E112-96)) In case of composites a correction to the linear intercept method proposed by Wurst [30] was applied. Hardness was determined by Vickers hardness tester MMT-3 (Buehler, Japan), a load of 1000 g was employed at a dwell time of 20 s. At least five measurements were performed at different locations of each pellet. The fracture toughness was calculated by the length of the cracks originating from the edges of the indentation marks, using the method described in-depth by Niihara et al. [31]. Ultrasonic measurement (both longitudinal and shear wave velocity) were conduced on each pellet to determine Young's modules (ASTM E494-92a).

The three-point bending strength tests (using an Instron 4505 apparatus, UK) were conducted in argon, for a loading speed of 0.5 mm min^{-1}. Measurements were done at room temperature and at 1600 °C. For this test, rectangular blocks ($2.5 \times 3 \times 20\ mm^3$) of sintered samples were cut by electric discharge machining and were polished on the lateral surfaces using diamond paste. The reported flexural strengths are the average of five specimens.

Electrical resistivity was measured at room temperature using a four linear probe method. The electrical resistivity measurements were carried out by inducing a current of 10 A in bar specimens $2.5 \times 3 \times 20\ mm^3$.

2.3. Sintering activation energy determination

Constant heating rate experiments were done to measure the activation energy value of titanium diboride for sintering process. Wang and Raj [32] have derived the sintering-rate equation (Eq. 1) used for the quantitative analysis of densification data measured by constant rate heating techniques, noting that the sintering-rate

$$\ln\left(T\frac{dT}{dt}\frac{dD}{dT}\right) = -\frac{Q_a}{RT} + \alpha_{V,B} \tag{1}$$

where

$$\alpha_{V,B} = \ln[f(D)] + \ln\frac{C\gamma V^{2/3}}{R} - N\ln G \tag{2}$$

Here, D is the density, R the gas constant, $f(D)$ a function only of density, C a constant, V the molar volume, γ surface energy, G the grain size, and N the grain size power law ($N=3$: lattice diffusion, $N=4$: grain-boundary diffusion).

Using shrinkage and density data measured at different heating rates, the activation energy Q_a value can be determined from the slope of the Arrhenius-type plot of $\ln\left(T\frac{dT}{dt}\frac{dDF}{dT}\right)$ versus $1/T$ at the same density, under a constant grain size.

This approach is similar to the combined-stage sintering model [33]. This model is based on the Herring's scaling law and assumes that grain size is independent of sample's density. Assuming that one diffusion mechanism prevails (i.e. grain boundary or volume diffusion) in the densification.

$$\ln\left(-\frac{TdL}{Ldt}\frac{dT}{dt}\right) = \ln\left(\frac{\gamma V_m D_{eff}}{R}\right) + \ln\left(\frac{\Gamma}{G^n}\right) - \frac{1}{T}\frac{Q_a}{R} \tag{3}$$

where Q_a corresponds to the apparent activation energy during sintering. Γ_b and Γ_v are scaling factors [33] for grain boundary

and volume diffusion respectively. D_{eff} and n are related to the dominant diffusion mechanism. If Γ and G are independent of density, plotting the left-hand side of Eq. (3) versus $1/T$ at a constant relative density for different heating rates (dT/dt) gives a line with a slope corresponding to $-Q/R$.

In the present work we use relative densities as a parameter to evaluate activation energy for sintering, although the relative shrinkage of specimens was also measured. For the calculations purposes the values used below correspond to the mean values of at least of five samples. We chose the densities interval of 70–85 of theoretical density suitable for calculations since the grain growth in this interval was minimal.

3. Results

3.1. Sintering

Apparent densities of microwave sintered samples as a function of sintering temperature at constant time of 10 min and heating rates of 5, 20 and 50 °C min^{-1} are plotted in Fig. 2. In case of microwave sintering of pure TiN, density quickly increases with sintering temperature until maximum density is reached at 1450 °C. In case of TiN–TiB_2 composites the density monotonically increases up to 1400 °C, which is followed by increase in densification rate until maximum density is achieved at 1600 °C.

The development of material microstructure as a function of microwave sintering temperature for pure TiB_2 is shown in SEM images (Fig. 3). The effect of composition at fixed temperature of 1600 °C and heating rate of 5 °C min^{-1} is shown in Fig. 4.

3.2. Sample characterizations

The hardness values we found in the present study (Table 1) are close to those usually reported in the literature for the TiB_2 ceramics (Table 2) [6–12,14,34]. It is interesting that an addition of less hard TiN phase favors the formation of more homogeneous and fine microstructure during sintering and causes an increase in hardness due to the grain refinement [35,36]. In case of 36 wt% TiB_2 composition the heating rate does not significantly influences materials properties.

In terms of fracture toughness the K_{IC} value for bulk TiB_2 is lower than that expected in bulk titanium diboride ceramics because the maximum plateau for mechanical properties in case of TiB_2 is 6–8 μm [37]. In case of composites, there is an increase in K_{IC} due to finer grain size and since the crack-deflection was found as primary strengthening mechanism further increase in fracture toughness requires introduction of whiskers or specific grain-boundary structure [35,36].

The values for electrical resistivity for pure TiN and TiB_2 agree reasonably with the available literature data [12,13,38]. In case of TiN–TiB_2 composites, the electrical resistivity decreases with increase in TiB_2 content similar to the rule of mixtures. Data for Young's modulus and bending strength measured at room temperature follow similar trend, and gradually increase with increase in TiB_2 content (Fig. 5).

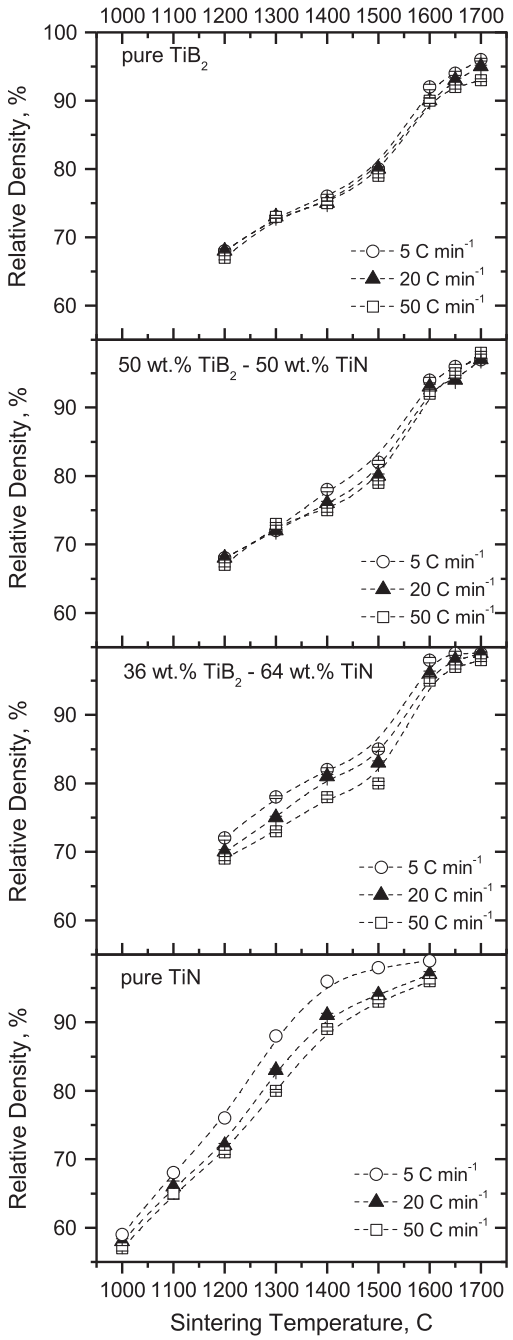

Fig. 2. Effect of heating rate, composition and sintering temperature on densification process during microwave sintering of ceramics in TiN–TiB_2 system.

3.3. Determination of the activation energy for sintering

Three different relative densities 70%, 75% and 80% have been used for the calculation of the activation energy for TiB_2 composites sintering (in case of 36 wt% TiB_2 composite densities of 75, 80 and 85% were used), corresponding to a range where no signification grain growth has yet occurred. The Arrhenius plot corresponding to relations (1 and 3) is presented in Fig. 6. The resulting average activation energy ranges from 850 ± 60 to 150 ± 13 kJ mol^{-1} (Fig. 7) in cases of pure TiB_2 and TiN, respectively.

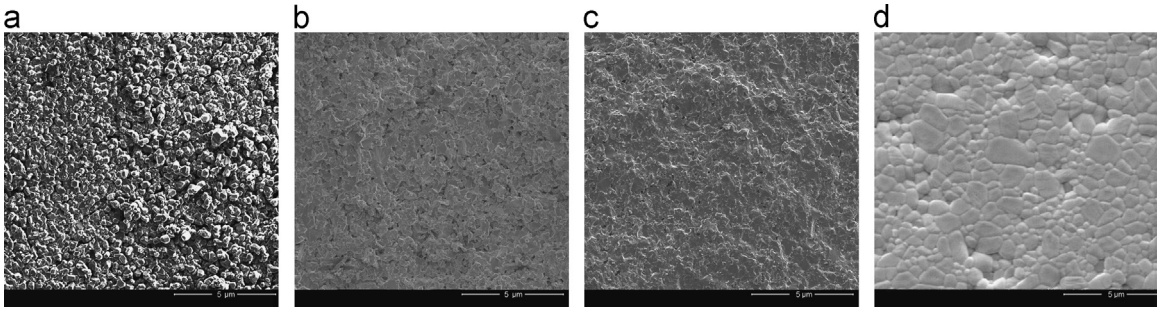

Fig. 3. Microstructure evolution during microwave sintering of nanocrystalline TiB_2 powder: (a) 1400 °C, (b) 1500 °C, (c) 1600 °C, and (d) 1650 °C.

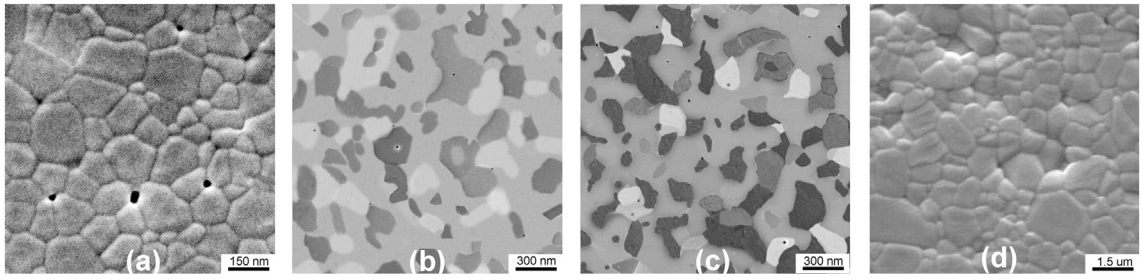

Fig. 4. Microstructure of ceramics of TiN–TiB_2 system after microwave sintering at 1650 °C and heating rate of 5 °C · min^{-1}: (a) TiN, (b) 36 wt% TiB_2, (c) 50 wt% TiB and (d) TiB_2. In (b) and (c) dark phase is TiB_2 and light phase is TiN.

Table 1
Processing parameters, microstructural characteristics and properties of microwave sintered composites.

Sample composition	T_{mws} (°C)	Heating rate (°C min^{-1})	Relative density (%)	Grain size (μm)	*Hv* (1.0 Gpa)	K_{IC} (MPa $m^{1/2}$)	*E* (Gpa)	Bending strength (3 point) (MPa)	Electrical resistivity, ρ (Ω cm × 10^{-6})
TiN	1500	5	99	0.24	18.2 ± 0.3	3.2 ± 0.1	430 ± 8	320 ± 13	20
36 wt% TiB_2	1650	5	99	0.23	26.2 ± 0.4	6.2 ± 0.34	440 ± 11	368 ± 15	14
36 wt% TiB_2	1650	20	98	0.22	25.3 ± 0.4	6.0 ± 0.24	435 ± 15	372 ± 13	13
36 wt% TiB_2	1700	50	98	0.31	24.6 ± 0.3	6.05 ± 0.17	432 ± 12	365 ± 15	13
50 wt% TiB_2	1700	20	97	0.25	25.6 ± 0.4	5.9 ± 0.11	450 ± 10	380 ± 16	13
TiB_2	1700	20	95	2.0	24 ± 0.6	5.58 ± 0.32	480 ± 10	400 ± 17	11

4. Discussion

4.1. Effect of TiN addition on sintering and microstructure

Addition of titanium nitride to the TiB_2 ceramics allowed to ensure highly homogeneous heating during microwave sintering of the composite. In fact titanium nitride is a natural microwave absorber due to metal-like conductivity at room temperature. And since the starting particle and agglomerate size was much smaller than 1 μm, the microwave heating occurred only by ohmic losses. This ensured high heating rate up to 800 °C without any adjustment of microwave heating power [20,25,39]. After this point the amount of TiN played major role in maximum power used in order to achieve desired heating rate and sintering temperature. To achieve heating rate of 20 °C · min^{-1} the microwave output power level in case of TiN, 36 wt% TiB_2, 50 wt% TiB_2 and pure TiB_2 was 20, 25, 30 and 35% of maximum load, respectively. Hence, even higher heating rates may be achieved similar to those usually used during SPS (> 200 °C min^{-1}) [9].

Homogeneous volumetric heating due to TiN addition allowed to preserve fine-grain structure (Fig. 4) up to temperatures as high as 1600 °C. However, in case of fine TiN starting powders the titanium nitride ceramics can be easily consolidate to full density even at 1500 °C. Hence, at higher temperatures in the TiN–TiB_2 compositions the grain-growth of TiN dominates. In this case the TiB_2 grains are at least twice smaller than those of TiN (Fig. 4). This increases both Vickers hardness and fracture toughness of composites.

In case of pure TiB_2, solid-bond necking forms between particles at temperatures as low as 800 °C. Since neck formation is not accompanied by shrinkage, this formation and further neck growth is believed to result from a surface-diffusion mechanism. Shrinkage is not observed for sintering temperatures less than 1200 °C. During this 400 °C interval large (~250 nm) grains are formed with faceted surfaces

Table 2
Summary of research illustrating the effect of different sintering additives on the mechanical and electrical properties of TiB_2 ceramics.

Sample composition (wt%)	Processing details Method/ temperature (°C/Dwell time) (min)	Relative density (%)	Grain size (μm)	*Hv* (GPa)	K_{IC}, (MPa $m^{1/2}$)	*E* (GPa)	Bending strength (MPa)	Electrical resistivity, ρ (Ω cm $\times 10^{-6}$)
TiB_2 [11]	SPS/1400/10	97.6	3	18.3 (±0.6)	5.8 (±0.8)	428	–	13.8
TiB_2 [12,13]	HP/1800/60	97.5	5	25–26	4.6 (±0.5)	497	–	15.1
TiB_2 [34]	CS/2200/60	99.4	3–50	–	5.0	510	232 3P	8.3
TiB_2 (this study)	MWS/1700/10	95.5	2	24 (±0.6)	5.58 (±0.32)	480 (±10)	400(±17) 3P	9
TiB_2-3 CrB_2 [14]	MWS/2100/30	98	4	27.0 (±1.3)	6.1 (±0.17)	–	–	–
TiB_2–3CrB_2 [14]	HP/2000/60	99	20	26.7 (±0.5)	4.78 (±0.57)	–	–	–
TiB_2–2.5 Ti [10]	SPS/1650/5	99.1	8	26.8 (±0.6)	5.9 (±0.3)	–	558 (±39) 4P	–
TiB_2–5$TiSi_2$ [5]	HP/1600/60	99.6	4	25.2 (±0.6)	5.8 (±0.5)	517 (±11)	425 (±68) 4P	10
TiB_2–10$TiSi_2$ [5]	HP/1600/60	99.6	6	23.5 (±1.0)	4.2 (±0.8)	470 (±15)	337(± ±67) 4P	9.9
TiB_2–5AlN [6]	HP 1800/60	98.0	4	22.0	6.8	450	650 4P	–
TiB_2–10Si_3N_4 [7]	HP/1800/60	96	3.8	20	4.4	–	400 4P	–
TiB_2–36TiN [8]	RHP/1850/30	98.0	2	18	5.8	–	390 3P	–
TiB_2–36TiN [9]	RSPS/1600/13	97.8	0.4	20.4 (±1.6)	5.05 (±0.17)	–	–	–
TiB_2–36TiN (this study)	MWS/1650/10	99.2	0.23	26.2 (±0.4)	6.20 (±0.34)	440 (±10)	368(±13) 3 P	14

Notes: MWS—microwave sintering, CS—conventional sintering, SPS—spark-plasma sintering, HP—hot-pressing, RHP—reactive hot-pressing, RSPS—reactive spark-plasma sintering; 4P—point bending strength, 3P—3 point bending strength.

(Fig. 2 (a)), which is another proof of active surface diffusion at low temperatures. This allows forming of TiB_2 ceramics without any secondary phases (e.g. TiB) at higher temperatures and thus providing an additional enhancement of bending strength and Young's modulus in particular [11]. After temperature of 1600 °C we experience formation of elongated grains in TiB_2, which is an indication of grain growth process. Hence the average grain size of fully-dense sample is close to 2 μm, which is enough to possess hardness and fracture toughness similar to the dense samples produced by hot-pressing.

4.2. Sintering mechanism

In case of sintering data with visible densification (i.e. > 1200 °C in case of TiB_2 ceramics) the consolidation process followed a shrinkage-producing mechanism (i.e. grain-boundary or volume diffusion) (Fig. 2). It is interesting to note that with increase in TiB_2 content the effect of heating rate on density becomes less important. Similar situation has been observed by Skorokhod and Krstic [40] during conventional sintering of B_4C–TiB_2 where it was attributed to the coarsing of very fine (~100 nm) TiB_2 particles in B_4C matrix.

Fig. 7 underlines decrease in activation energy for sintering with increase in TiN content. This suggests that different diffusing species were active for pure TiN and TiB_2. Moreover, data for pure TiN $Qa = 150 \pm 13$ kJ mol^{-1} is close to results of Demirskyi et al. [41] of 230 kJ mol^{-1} that was determined for the grain-growth in nanocrystalline TiN powder occurred mainly by grain-boundary diffusion. Whereas in case of volume diffusion for conventional sintering the value of 480–520 kJ mol^{-1} is usually reported [41–43].

In case of TiB_2 the data on activation energy of diffusion is sparse. Baumgartner et al. [34] reported an activation energy for the grain-growth for TiB_2 of 1020 ± 230 kJ mol^{-1}, but they did not specify diffusion mechanism or diffusing species. During consolidation of fine TiB_2 powder using conventional sintering at 1800–2100 °C Ouabdesselam et al. [44] reported a value of 774 ± 46 kJ mol^{-1} in case of the densification process at by a volume diffusion mechanism.

Moreover, the activation energies for the diffusion of B in TiB or TiB_2 are reported to be ~190 kJ mol^{-1} [45], which is associated with vacancy diffusion process and is much smaller than the estimated activation energy for sintering for TiB_2 in the present study. Therefore the boron diffusion in TiB_2 is not the rate-controlling factor during microwave sintering.

Further, the activation energy for the self-diffusion of titanium in TiC is 770 kJ mol^{-1} [46]. Here the diffusion process would be rate-limited by the slowest diffusing species, which, for TiB_2, is likely to be the titanium atoms, as is the case for TiC. This provides a good agreement with data on grain-growth by Baumgartner et al. [34] and on densification by Ouabdesselam et al. [44]. For this reason we believe that in case of composites with TiB_2 the Ti diffusion in TiB_2 is the

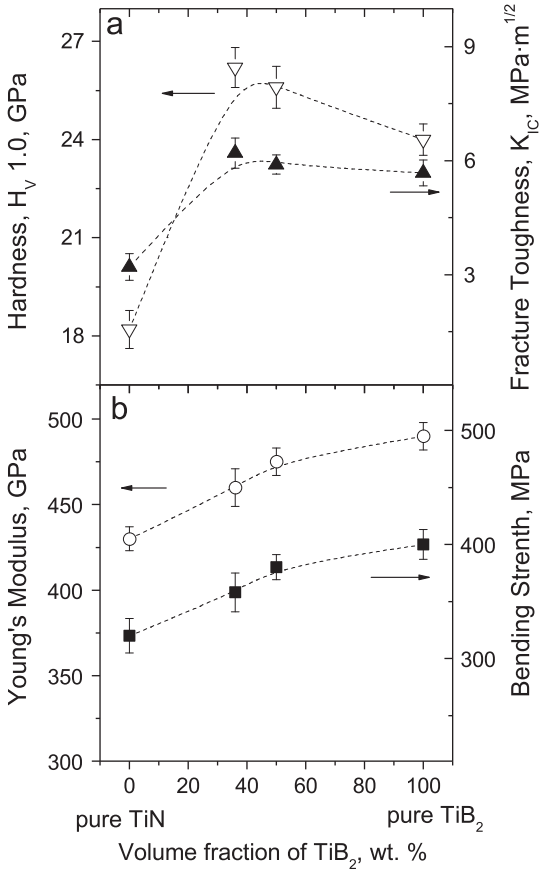

Fig. 5. Effect of composition on mechanical properties of ceramics in TiN–TiB_2 system after microwave sintering: (a) Vickers hardness and K_{IC}; (b) Young's modulus and 3-point bending strength.

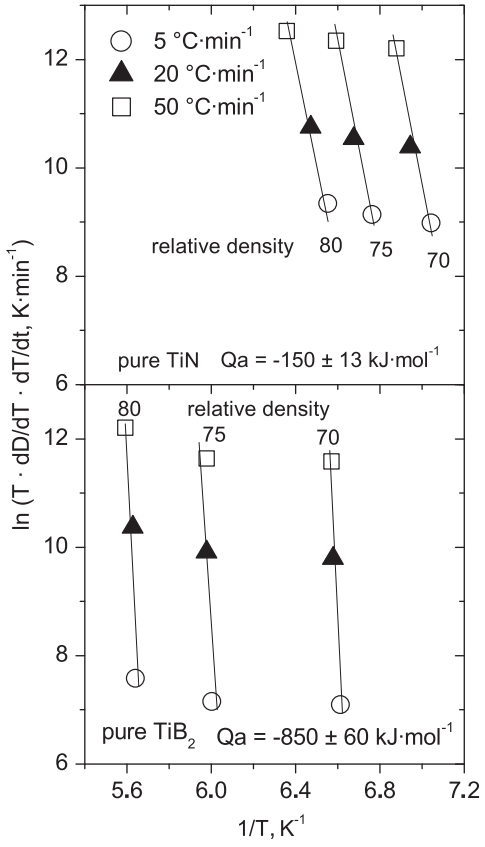

Fig. 6. Linear regression for determination of the activation energy of the microwave sintering process of pure TiN and TiB_2 ceramics with combined stage sintering model assuming a constant grain size.

rate controlling factor. In case of 36 wt% TiB_2 composite both N diffusion in TiN and Ti diffusion in TiB_2 contribute at the same time to densification process.

Hence, in this case much faster densification rate is achieved. In terms of hardness and K_{IC} this composite has better properties than bulk TiB_2 specimens (Table 1), and it is much easier to consolidate by pressureless microwave sintering than SPS.

5. Conclusions

A study of the pressureless microwave sintering of nanocrystalline TiN–TiB_2 system has been presented. High densification of green compacts has been achieved with addition of TiN as a secondary phase to insure homogeneous heating during sintering. The estimated activation energies indicated a nitrogen diffusion in TiN and Ti diffusion in TiB_2 as the rate-controlling factors for sintering. The sintered samples present a relative density of $>95\%$ in case of TiB_2 and fully dense when ceramics with TiN have been used. Densification process for TiB_2 ceramics was enhanced by addition of TiN. The TiB_2 composites sintered at 1650–1700 °C provide the attractive combination of dense uniform microstructure and excellent mechanical properties, including relative density $>99\%$, a Vickers hardness of 26.2 ± 0.4 GPa, bending strength of 368 ± 15 MPa, Young's modulus of 440 ± 11 GPa and a fracture toughness of

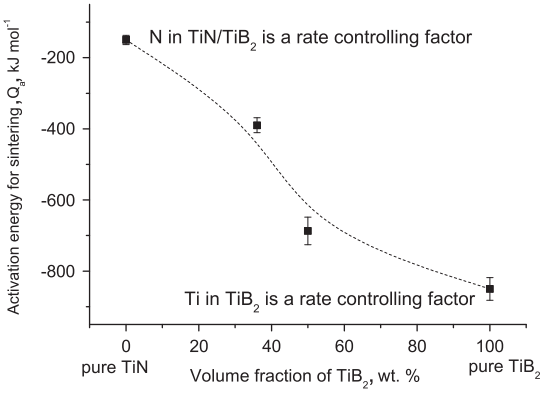

Fig. 7. Effect of TiB_2 content on activation energy for microwave sintering in TiN–TiB_2 system.

6.2 ± 0.34 MPa m$^{1/2}$. The dense and fine-grained microstructures are the main factors to improve the mechanical properties of ceramics consolidated by microwave sintering.

Acknowledgments

One of the authors (D.D.) was supported by a grant # 67/H12 "Sintering kinetics of nanocrystalline ceramics in the external electric and microwave fields" and III-2012 (Ц) "Development of nanocomposites in Ti–Zr–Al–B–N system using field-assisted sintering."

Thanks are due also to Dr. Jiping Cheng (PSU) for technical assistance during microwave sintering experiments.

References

[1] R.G. Munro, Material properties of titanium diboride, Journal of Research of the National Institute of Standards and Technology 105 (2000) 709–720.

[2] B. Basu, G.B. Raju, A.K. Suri, Processing and properties of monolithic TiB_2-based materials, International Materials Review 51 (2006) 352–374.

[3] R. Konigshofer, S. Furnsinn, P. Steinkellner, W. Lengauer, R. Haas, K. Rsbitsch, M. Scheerer, Solid-state properties of hot-pressed TiB_2 ceramics, International Journal of Refractory Metals and Hard Materials 23 (2005) 350–357.

[4] J.H. Park, Y.H. Lee, Y.H. Koh, H.E. Kim, S.S. Baek, Effect of hot-pressing temperature on densification and mechanical properties of titanium diboride with silicon nitride as a sintering aid, Journal of the American Ceramic Society 83 (2000) 1542–1544.

[5] G.B. Raju, B. Basu, Densification, sintering reactions, and properties of titanium diboride with titanium disilicide as a sintering aid, Journal of the American Ceramic Society 90 (2007) 3415–3423.

[6] L.-H. Li, H.-E. Kim., E.S. Kang, Sintering and mechanical properties of titanium diboride with aluminum nitride as a sintering aid, Journal of the European Ceramic 22 (2002) 973–977.

[7] J.-H. Park, Y.-H. Koh, H.-E. Kim, C.S. Hwang, Densification and mechanical properties of titanium diboride with silicon nitride as a sintering aid, Journal of the American Ceramic Society 82 (1999) 3037–3042.

[8] G. Zhang, Z. Jin, X. Yue, TiN–TiB_2 composites prepared by reactive hot pressing and effects of Ni addition, Journal of the American Ceramic Society 78 (1995) 2831–2833.

[9] I. Khobta, O. Petukhov, O. Vasylkiv, Y. Sakka, A. Ragulya, Synthesis and consolidation of TiN/TiB_2 ceramic composites via reactive spark plasma sintering, Journal of Alloys and Compounds 509 (2011) 1601–1606.

[10] Z.-H. Zhang, X.-B. Shen, F.-C. Wang, S.-K. Lee, Q.-B. Fan, M.-S. Cao, Low-temperature densification of TiB_2 ceramic by the spark plasma sintering process with Ti as a sintering aid, Scripta Materialia 66 (2012) 167–170.

[11] A. Mukhopadhyay, T. Venkateswaran, B. Basu, Spark plasma sintering may lead to phase instability and inferior mechanical properties: a case study with TiB_2, Scripta Materialia 02 (2013) 027, http://dx.doi.org/10.1016/j.scriptamat.

[12] T.S.R.Ch Murthy, B. Basu, R. Balasubramaniam, A.K. Suri, C. Subramanian, R.K. Fotedar, Processing and properties of TiB_2 with $MoSi_2$ sinter-additive: a first report, Journal of the American Ceramic Society 89 (2006) 131–138.

[13] A. Mukhopadhyay, G.B. Raju, B. Basu, A.K. Suri, Correlation between phase evolution, mechanical properties and instrumented indentation response of TiB_2-based ceramics, Journal of the European Ceramic Society 29 (2009) 505–516.

[14] C.E. Holcombe, N.L. Dykes, Microwave sintering of titanium diboride, Journal of Materials Science 26 (1991) 3730–3738.

[15] D. Agrawal, Microwave sintering of ceramics, composites, metals, and transparent materials, Journal of Materials Education 19 (1999) 49–58.

[16] D.K. Agrawal, Microwave processing of ceramics: a review, Current Opinion in Solid State and Materials Science 3 (1998) 480–486.

[17] O. Vasylkiv, D. Demirskyi, Y. Sakka, A. Ragulya, H. Borodianska, Densification kinetics of nanocrystalline zirconia powder using microwave and spark plasma sintering—a comparative study, Journal of Nanoscience and Nanotechnology 12 (2012) 4577–4582.

[18] D. Demirskyi, H. Borodianska, S. Grasso, Y. Sakka, O. Vasylkiv, Microstructure evolution during field-assisted sintering of zirconia spheres, Scripta Materialia 65 (2011) 683–686.

[19] M.A. Janney, H.D. Kimrey, M.A. Schmidt, J. Kiggans, Grain growth in microwave-annealed alumina, Journal of the American Ceramic Society 74 (1991) 1675–1681.

[20] D. Demirskyi, D. Agrawal, A. Ragulya, Densification kinetics of powdered copper under single-mode and multimode microwave sintering, Materials Letters 64 (2010) 1433–1436.

[21] D. Demirskyi, D. Agrawal, A. Ragulya, Neck growth kinetics during microwave sintering of nickel powder, Journal of Alloys and Compounds 509 (2011) 1790–1795.

[22] D. Demirskyi, D. Agrawal, A. Ragulya, Neck formation between copper spherical particles under single-mode and multimode microwave sintering, Materials Science and Engineering A 527 (2010) 2142–2145.

[23] D. Demirskyi, D. Agrawal, A. Ragulya, Neck growth kinetics during microwave sintering of copper, Scripta Materialia 62 (2010) 552–555.

[24] R. Roy, D. Agrawal, J. Cheng, S. Gedevanishvili, Full Sintering of powdered-metal bodies in a microwave field, Nature 399 (1999) 668–670.

[25] M. Oghbaei, O. Mirzaee, Microwave versus conventional sintering: a review of fundamentals, advantages and applications, Journal of Alloys and Compounds 494 (2010) 175–189.

[26] D. Demirskyi, A. Ragulya, D. Agrawal, Initial stage sintering of binderless tungsten carbide powder under microwave radiation, Ceramics International 37 (2011) 505–512.

[27] D. Demirskyi, H. Borodianska, D. Agrawal, A. Ragulya, Y. Sakka, O. Vasylkiv, Peculiarities of the neck growth process during initial stage of spark-plasma, microwave and conventional sintering of WC spheres, Journal of Alloys and Compounds 523 (2012) 1–10.

[28] C. Plapcianu, A. Agostino, P. Badica, G.V. Aldica, E. Bonometti, G. Ieluzzi, S. Popa, M. Truccato, S. Cagliero, Y. Sakka, O. Vasylkiv, R. Vidu, Microwave synthesis of fullerene-doped MgB_2, Industrial a Engineering Chemistry Research 51 (2012) 11005–11010.

[29] P.G. Karandikar, M.K. Aghajanian, D. Agrawal, J. Cheng, Microwave assisted (mass) processing of metal-ceramic and reaction bonded composites, in: R. Tandon (Ed.), Proceedings of the Ceramic Engineering and Science, Mechanical Properties and Performance of Engineering Ceramics and Composites II, vol. 27, no. 2, American Ceramic Society, 2007 pp. 435–446.

[30] J.C. Wurst, J.A. Nelson, Linear intercept technique for measuring grain size in two-phase polycrystalline ceramics, Journal of the American Ceramic Society 55 (1972) 109.

[31] K. Niihara, R. Morena, D.P.H. Hasselman, Evaluation of KIC of brittle solids by the indentation method with low crack-to-indent ratios, Journal of Materials Science Letters 1 (1982) 13–16.

[32] J. Wang, R. Raj, Estimate of the activation energies for boundary diffusion from rate-controlled sintering of pure alumina, and alumina doped with zirconia or titania, Journal of the American Ceramic Society 73 (1990) 1172–1175.

[33] J.D. Hansen, R.P. Rusin, M.-H. Teng, D. Lynn Johnson, Combined-stage sintering model, Journal of the American Ceramic Society 75 (1992) 1129–1135.

[34] H.R. Baumgartner, R.A. Steiger, Sintering and properties of titanium diboride made from powder synthesized in a plasma-arc heater, Journal of the American Ceramic Society 67 (1984) 207–212.

[35] A.V. Ragulya, V.V. Skorokhod, Consolidated Nanostructured Materials, Naukova Dumka, Kiev, 2007.

[36] R.A. Andrievski, A.M. Glezer, Strength of nanostructures, Physics Uspekhi 52 (2009) 315–358 in Russian.

[37] R.W. Rice, Grain size and porosity dependence of ceramic fracture energy and toughness at 22 °C, Journal of Materials Science 31 (1996) 1969–1983.

[38] T. Graziani, A. Bellosi, Densification and characteristics of TiN ceramics, Journal of Materials Science 14 (1995) 1078–1081.

[39] D. Demirskyi, A. Ragulya, Low-temperature microwave sintering of TiN–SiC nanocomposites, Journal of Materials Science 47 (2012) 3741–3745.

[40] V. Vl., V.D. Skorokhod, Krstic, processing, microstructure, and mechanical properties of B_4C–TiB_2 particulate sintered composites Part I, Pressureless Sintering and Microstructure Evolution, Powder Metallurgy and Metal Ceramics 39 (2000) 414–423.

[41] D. Demirskyi, A. Ragulya, Grain growth kinetics during microwave sintering of the nanocrystalline titanium nitride. In: O. Fesenko, L. Yatsenko, M. Brodin (Eds.), Nanomaterials Imaging Techniques, Surface

Studies, and Applications, Springer. Springer Proceedings in Physics 146, http://dx.doi.org/10.1007/978-1-4614-7675-7_16. 2013 in press.
[42] M.A. Kuzenkova, P.S. Kislyi, Vacuum sintering of titanium nitride, Powder Metallurgy and Metal Ceramics 10 (1971) 125–128.
[43] F. Anglezio-Abautret, B. Pellissier, M. Miloche, P. Eveno, Nitrogen self-diffusion in titanium nitride single crystals and polycrystals, Journal of the European Ceramic Society 8 (1991) 299–304.
[44] M. Ouabdesselam, Z.A. Munir, The sintering of combustion-synthesized titanium diboride, Journal of Materials Science 22 (1987) 1799–1807.
[45] H. Schmidt, G. Borchardt, C. Schmalzried, R. Telle, S. Weber, H. Scherrer, Self-diffusion of boron in TiB_2, Journal of Applied Physics 93 (2003) 907–911.
[46] S. Sarian, Anomalous diffusion of 14C in $TiC_{0.67}$, Journal of Applied Physics 39 (1968) 5036–5041.